Correlations between the mechanical loss and atomic structure of amorphous TiO_2 doped Ta_2O_5 coatings

R. Bassiri[a,b,*], K. Evans[a], K. B. Borisenko[c], M. M. Fejer[b], J. Hough[a], I. MacLaren[a], I. W. Martin[a], R. K. Route[b], S. Rowan[a]

[a] *SUPA, School of Physics and Astronomy, University of Glasgow, University Avenue, Glasgow G12 8QQ, United Kingdom*
[b] *E. L. Ginzton Laboratory, Stanford University, Stanford, California 94305, USA*
[c] *Department of Materials, University of Oxford, Parks Road, Oxford OX1 3PH, United Kingdom*

Abstract

Highly reflective dielectric mirror coatings are critical components in a range of precision optics applications including frequency comb techniques, optical atomic clocks, precision interferometry and ring laser gyroscopes. A key limitation to the performance in these applications is thermal noise, arising from the mechanical loss of the coatings. The origins of the mechanical loss from these coatings is not well understood.

Recent work suggests that the mechanical loss of amorphous Ta_2O_5 coatings can drop by as much as 40 % when it is doped with TiO_2. We use a combination of electron diffraction data and atomic modeling using molecular dynamics to probe the atomic structure of these coatings, and examine the correlations between changes in the atomic structure and changes in the mechanical loss of these coatings. Our results show the first correlation between changes in the mechanical loss and experimentally measured changes in the atomic structure resulting from variations in the level of TiO_2 doping in TiO_2 doped Ta_2O_5 coatings, in that increased homogeneity at the nearest neighbour level appears to correlate with reduced mechanical loss. It is demonstrated that subtle but measurable changes in the nearest neighbour homogeneity in an amorphous material

*Corresponding author
Email address: rbassiri@stanford.edu (R. Bassiri)

can correlate with significant changes in macroscopic properties.

1. Introduction

High performance dielectric mirror coatings that have low optical and mechanical loss are required for use in ring laser gyroscopes [1], frequency comb techniques [2], optical clocks [3] and precision interferometry [4].

One of the most important limits to the achievable performance in such high precision optical applications is thermal noise, the magnitude of which is related to the mechanical loss in the coating materials [5]. The mechanical loss (or internal friction) can be probed by precision measurements of the quality factor of mechanical resonances [6]. Dielectric mirrors are typically formed from stacks of alternating layers of materials with high and low refractive indices, where Ta_2O_5 (tantala) and SiO_2 (silica) have often been the materials of choice.

Previous work has suggested that the mechanical loss of tantala coatings can be reduced by up to 40 % by doping with TiO_2 (titania) [7]. It has also been shown that the loss of tantala is temperature dependent [8], and that the temperature dependence of the loss in pure and titania doped tantala coatings is strongly dependent on post-deposition heat-treatment, with several low-temperature mechanical loss peaks emerging as the heat-treatment temperature is increased [8, 9].

It has been postulated that these observed changes in the mechanical loss are related to structural and chemical changes at the atomic scale, although the details of these changes have not, as yet, been identified. This paper presents the first observations of a correlation between changes in the mechanical loss and experimentally measured changes in the atomic structure resulting from varying the titania doping content in tantala coatings.

2. Experimental and Theoretical Methods

The coatings studied in this work are multi-layer coatings deposited by ion-beam sputtering consisting of 30 alternating layers of $\lambda/4$ (at 1.064 μm) thick

SiO_2 and Ta_2O_5 doped with TiO_2 deposited on fused silica blanks, manufactured by LMA (LMA, CNRS-IN2P3, France). There were two different coating chambers used during the manufacturing process; a larger chamber that uses two radio frequency ion sources, and a smaller chamber that has a Kaufman source with tungsten filaments which heat both the target and the substrate. The level of TiO_2 doping in the coatings is expressed as a Ti cation percentage throughout this paper, and for simplicity, TiO_2 doping is denoted simply as Ti doping; the doping concentrations were 0, 8.3, 20.4, 25.7, 28.3, 53.8 % (cation) Ti as determined using Electron Energy Loss Spectroscopy (EELS). The $0, 8.3, 20.4, 28.3$ % doped coatings were deposited in the smaller coating chamber and the 25.7 and 53.8 % doped coatings were deposited in the larger coating chamber. All coatings were heat-treated after deposition at 600 °C in air for 24 hours. Further details of the deposition process can be found in the literature for these coatings [7], and ion-beam sputtering in general [10].

The coating mechanical loss has been measured previously as described by Harry et al. [7]. As these are multi-layer coating mechanical loss measurements, the mechanical loss values stated by Harry et al. [7] include the loss associated with the SiO_2 component, as well as the loss associated with the Ti doped Ta_2O_5 component. However, any changes in the mechanical loss can be assumed to be the result of the changes to the Ti doping concentration, as this is the most significant variable during the manufacturing process. The extracted mechanical loss of the Ti doped Ta_2O_5 component of these coatings is used in the results presented in Section 3. The process for extraction has been previously described by Crooks et al. [11], and the properties used for this calculation are listed in the Supplementary material.

Cross sections of the multilayers were prepared for transmission electron microscopy studies using a standard method. The samples were thinned using a Gatan Precision Ion Polishing System (PIPS) (Gatan Inc., Pleasanton, CA, USA), which used Ar^+ ion irradiation at a relatively low energy, 4 kV beam, and a final 0.5 kV 'polishing' stage, to avoid any changes to the sample material structure [12]. They were then characterized in a FEI Tecnai T20 Transmission

Electron Microscope (TEM) (FEI Corp, Eindhoven, The Netherlands), operated with an accelerating voltage of 200 kV. Images and diffraction patterns were recorded using a SIS Megaview III CCD camera (Olympus SIS GmbH, Garching, Germany) . Electron diffraction patterns, recorded with a convergence semi-angle of $\alpha = 1.89$ mrad, were collected from suitably thin areas, to allow for adequate electron transmission of the tantala layers and then used in the subsequent analysis. The diffraction patterns were azimuthally averaged out to at least $q = 10$ Å^{-1}, this then being used as the raw data for calculating the reduced scattering intensities and Reduced Density Functions (RDFs). The RDF is computed by the Fourier transform of the averaged reduced scattering intensity and gives a statistical distribution of atoms in the material with regards to a central atom. The full details of the analytical procedures used for the calculation from experimental diffraction data have already been described in detail elsewhere [13, 14].

Full details of our modelling procedure can be found in Ref. [13] but a short summary is given here for the benefit of the reader. Initial models of the structure are constructed using the measured stoichiometry from EELS and the density from either physical density measurements or X-ray reflectometry to provide the correct number of atoms in a box of fixed size, resulting in a box of about 100 atoms in random positions. The atomic structure is then refined using a reverse Monte-Carlo (RMC) procedure to match the observed RDF whilst maintaining realistic interatomic distances. Following this, a density functional theory (DFT) molecular dynamics (MD) simulation of melting and rapid cooling is performed using the CASTEP package to ensure that all the atoms sit in physically reasonable positions. This utilizes the norm-conserving pseudopotentials of Lee et al. provided with the software [15] within the generalized gradient approximation (GGA) using the Perdew-Burke-Ernzerhof (PBE) exchange-correlation functional [16] where an energy cut off was set at 200 eV. The computed cell parameters were found to be within 1% of the experimental values for the 200 eV cutoff which was selected for the MD simulations. All models were first simulated at 3000 K, and then equilibrated at 2000 K. The

obtained models were then cooled down to 500 K in steps of 300 K. Finally, the structure was equilibrated at 300 K. At each temperature step, the structure was allowed sufficient time to find an equilibrium.

The time step in all simulations was 2 fs and total simulation time was around 20 ps for each of the tested models. It can be anticipated that a number of high frequency vibrational modes (for example, bond stretching vibrations) may not be well described by the selected relatively long integration time step. It is, however, a better suited option to describe atomic diffusion in the process of liquid quenching. It is our experience that diffusion facilitates the formation of the local structures in the simulations. In fact, if crystallisation is taken as analogy of local structure formation in amorphous solids during liquid quench, for some organic materials it was indeed observed that self-diffusion coefficient correlates well with crystal growth rates [17]. An implementation of the Nose-Hoover thermostat [18] was used in the simulations to control the temperature. The electron density was sampled only at the gamma point, which not only speeds up the simulations but is a reasonable approximation for an insulator. The simulations were performed in the canonical ensemble with periodic boundary conditions and a fixed lattice constant. To better understand the amorphous TiO_2 doped Ta_2O_5 structures over a longer range, a final large model for RMC refinement was then prepared by assembling together 27 randomly oriented small models obtained from the MD simulations of liquid quenching. This model was then refined using a small 0.1 Å maximum displacement step per iteration in the RMC routine, to preserve the simulated bond length and angle distributions as much as possible, while at the same time fitting the model to the experimental diffraction data and avoiding any un-physically short distances.

3. Correlations between Structural Parameters and Mechanical Loss Measurements

The averaged RDFs for the doped Ta_2O_5 coatings are shown in Fig. 1, where each RDF is the average of at least 10 RDFs from separate diffraction patterns collected from different locations in each coating. It should be noted that the

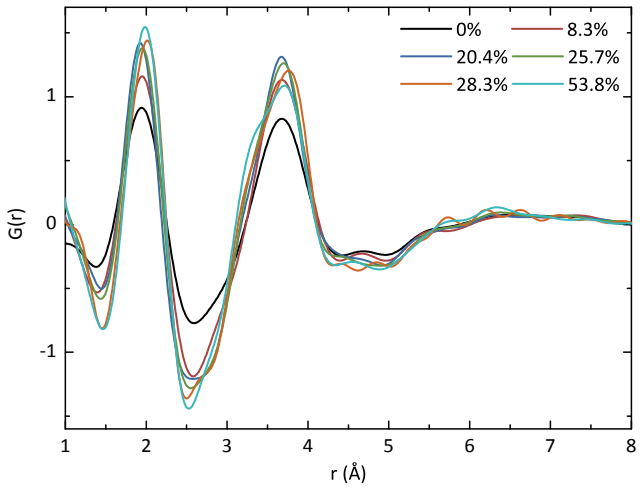

Fig. 1: Experimental RDFs for the Ta_2O_5 coatings doped with TiO_2 for the full range of Ti doping levels.

first major peak in the RDF at around 2 Å corresponds well to Ta-O and Ti-O distances in many tantalum or titanium oxides [19–21]. The second major peak was shown in previous work [13] to correspond to Ta...Ta distances, and by extension in this work is expected to correspond to Ta...Ta, Ta...Ti and Ti...Ti distances. Fig. 1 clearly shows a composition dependent variation in the RDF, meaning that the short-range atomic structure is changing significantly as the Ti doping concentration increases. Most notably, the first peak increases in height and decreases in width with increasing Ti content indicating increased homogeneity in the nearest neighbour bonds as Ti doping concentration increases. The second peak shows increased height but also a change in shape (especially at the highest Ti content), which may indicate an increased homogeneity from the nearest neighbor distances that make up this peak, and possibly some differentiation between the different types of metal...metal distances. A possible reason for such differentiation may be an increased clustering of tantala and titania oxides.

The changes in the RDFs as a consequence of Ti addition were tracked by statistical analysis of the RDFs including the positions, heights and widths of the two main peaks. The full analysis of these trends is included in the

Supplementary material. Changes in three of the analyzed parameters with composition show a clear correlation to changes in mechanical loss, as shown in Fig. 2. As is seen in Fig. 1, there is a small but discernible movement of the first peak and so Fig. 2 (a) shows the variation of first peak position with Ti content. Similarly, Fig. 2 (b) plots the position of the second peak in the RDFs. Interestingly, both the first and second peak positions show similar patterns of change with increasing Ti doping, both achieving maximum values for the 28.3% Ti coating. It appears that the metal-oxygen and metal...metal distances are furthest apart in the 28.3% Ti coating. Fig. 2 (c) shows a clear trend for the first peak to become sharper with increasing Ti content.

The correlation between the dependence of mechanical loss and metal-oxygen distances (first peak position) on titanium content is also illustrated in Fig. 2 (a). It shows that the first peak position is at its maximum of around 2 Å at the same point as the mechanical loss is at its minimum for the 28.3% Ti coating, although other points are seen at which the correlation is not so good. There is a similar pattern for the second RDF peak positions shown in Fig. 2 (b), with the maximum peak position of around 3.74 Å again at the minimum mechanical loss given by the 28.3% Ti coating. Remarkably, as the Ti doping increases both the first and second peak positions follow a somewhat similar trend, where before and after the 28.3% Ti doping level the peak positions are at a shorter distance and the mechanical loss is higher. Fig. 2 (c) indicates that the first peak full width at half maximum (FWHM) shows a particularly strong correlation to the mechanical loss with a very good match between the dependence of the two parameters on Ti content. This shows that in general as the peak becomes narrower and more well defined, the mechanical loss is also reduced. To demonstrate this correlation better, Fig. 2 (d) shows a plot of the FWHM of the first peak against the mechanical loss. As can be seen, there is a well defined linear correlation with a Pearson correlation coefficient of 0.93 between the mechanical loss and the FWHM of the first peak, thus demonstrating that an increased level of homogeneity at the nearest neighbour level for the metal-oxygen distances is correlated to minimal value of mechanical loss.

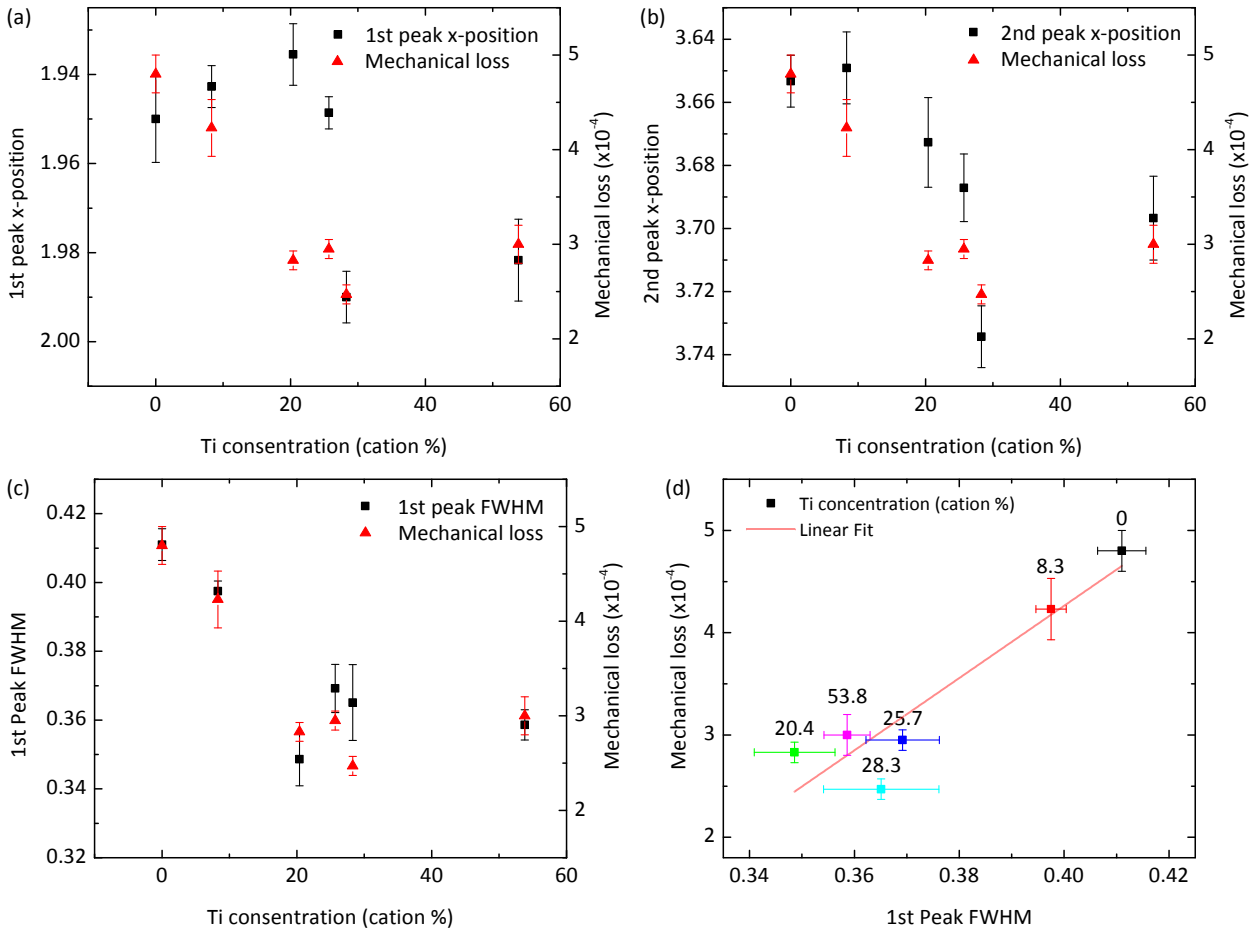

Fig. 2: RDF parameter statistics overlayed with the extracted tantala coating mechanical loss against the Ti doping concentrations: (a) Position of the first peak (metal-oxygen distances); (b) Position of the second peak (metal...metal distances); (c) Full width at half maximum (FWHM) of the first peak; (d) Linear correlation between changes in the FWHM of the 1st peak in the RDFs and the mechanical loss of the TiO_2 doped Ta_2O_5 coatings.

Coating	Stoichiometry (Ta:Ti:O)
20.4% Ti	0.26:0.06:0.68
53.8% Ti	0.17:0.20:0.63

Table 1: EELS stoichiometries for the 20.4% and 53.8% Ti doped Ta_2O_5 coatings

4. Modeling the variation of atomic structure with composition

In order to accurately probe the atomic structure further and gain a fuller understanding of the information stored in the RDF, atomic models were created for the 20.4% and 53.8% Ti doped Ta_2O_5 coatings. These concentrations of Ti doping were chosen because they were the only doped Ta_2O_5 coatings to have experimentally measured densities at the time of creating the models, which were 7.01 g/cm^3 for 20.4% Ti doped coating and 5.50 g/cm^3 for the 53.8% Ti doped coating. Experimental stoichiometries measured from EELS data were also used as inputs to these models, and are shown in Table 1. The structure of an undoped Ta_2O_5 coating has previously been modelled [13].

There are relatively few publications on Ta, Ti mixed oxides but those that exist suggest that Ti can substitute for Ta, although it modifies the structure of the oxide as it does so [22–24]. Furthermore, it is already known that Ti ions are of a similar size to Ta ions resulting in similar lengths for Ti-O and Ta-O bonds in Ti and Ta oxides and other compounds. Therefore, Ti atoms were given identical constraints to Ta atoms on positions relative to other Ti, Ta or O atoms in the model, for the purposes of the RMC refinement process.

Partial RDFs computed from the models refined using the combined RMC and DFT approach for the 20.4% and 53.8% Ti doped coatings can be found in Fig. 3. Fig. 3 (a) shows that, for the 20.4% Ti coating, the first major peak occurring at around 2 Å in the RDF is comprised of metal to oxygen bonds, which is dominated by Ta-O bonded distances with a small contribution from Ti-O bonded distances. There is then a small contribution from O...O distances at around 2.7 Å. In the region of 3 to 4.5 Å, metal to metal distances are dominant with a significant contribution from Ta...Ti distances and the largest contribution from Ta...Ta distances. There is also a very small contribution

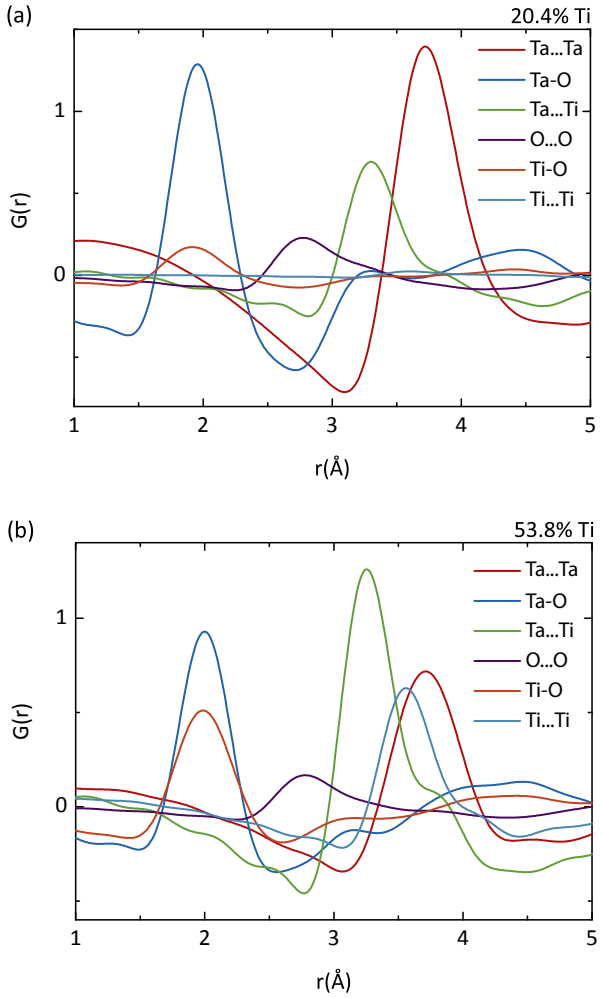

Fig. 3: Partial RDFs obtained from the combined RMC and DFT model for the (a) 20.4% and (b) 53.8% Ti doped coatings.

from Ti...Ti distances at around 3.6 Å and some longer range contributions from Ta...O non-bonded distances at around 4.5 Å. The dominant contributions in the partial RDF are from the Ta-O and Ta...Ta distances with smaller contributions from atom to atom distances involving Ti, as would be expected given the relatively small amount of Ti dopant in the coating and lower atomic number of Ti.

The 53.8% Ti coating has a much larger contribution from interatomic distances involving Ti atoms, as expected. As seen in Fig. 3 (b) Ta-O bonds and a larger contribution from the Ti-O bonds from 1.5 to 2.4 Å form the major contributions to the first peak in the experimental RDF. The second major peak in the experimental RDF has contributions from interatomic distances between 3 and 4 Å. It is apparent that this peak is wider than the one in the RDF of the 20.4% Ti coating, based on the larger contribution from the Ti...Ta distances at 3.3 Å with other major contributions from Ti...Ti distances at 3.6 Å and Ta...Ta distances at 3.8 Å. The Ti...Ti distances also have a much more noticeable contribution in the 53.8% Ti coating with a reduction in the contribution from the Ta...Ta distances, as can perhaps be expected given the much larger Ti dopant concentration.

Analyzing the refined models, a number of short Ta...Ta and Ta...Ti distances can be found, with some of the distances being considerably shorter than the sum of the respective covalent radii (Ta = 1.7 Å, Ti = 1.6 Å). It is not possible at present to firmly identify such distances as bonded or non-bonded ones. Analysis of the electron density distribution in the corresponding fragments is in progress and will be reported in the future. Nevertheless, defining the bonds as an interatomic distance of less than the sum of the corresponding atoms' covalent radii (O = 0.73 Å) and a bond tolerance parameter set at 0.1 Å, we can perform an analysis of bond type and bond angle distributions for the 20.4 % and 53.8 % Ti models. We included possibly non-bonded short Ta...Ta and Ta...Ti distances into the analysis.

The average bonded and non-bonded short distances for the two coatings are shown in Table 2. The results show that the average of such distances remain

Distance	**20.4% Ti**	**53.8% Ti**
Ta...Ta	3.75 ± 0.18	3.73 ± 0.19
Ta...Ti	3.29 ± 0.10	3.26 ± 0.11
Ta-O	2.00 ± 0.16	2.02 ± 0.12
Ti-O	1.97 ± 0.17	2.01 ± 0.15

Table 2: Average short interatomic distances (Å) for 20.4% and 53.8% Ti coatings

relatively constant between the coatings and that they correspond well to the major peaks distance distributions shown in the partial RDFs (Fig. 3). This also highlights that on average the Ta...Ti distances are around 0.5 Å shorter than Ta...Ta distances.

Fig. 4 (a) shows the comparison for bonded and non-bonded distance type distribution and shows that Ta...Ta distance contribution stays relatively constant between the Ti doping levels. The Ta-O bonds show a decrease in proportion as the Ti doping increases, as expected due to the increased proportion of titania in the atomic structure, subsequently causing an increase in the level of Ta...Ti distances and Ti-O bond contributions.

The angle type distributions shown in Fig. 4 (b) reflect the changes observed in the bonded and non-bonded distance type distributions, with fewer contributions from the angles that involve Ta-O bonds and an increase in Ti-O bonds as the Ti doping level increases. This is most noticeable when examining the O-Ta-O and O-Ti-O angle distributions. In the same way Ta-O-Ta decreases whilst Ti-O-Ti and Ti-O-Ta increase with increasing Ti content.

In both of the doped Ta_2O_5 models there were considerable contributions from the Ta_2O_2 ring fragments, that were previously seen in the heat-treated Ta_2O_5 coatings [13]. Fig. 5 (a) shows the DFT model for the 20.4% Ti coating, highlighting the presence of the Ta_2O_2 ring fragment (Fig. 5 (b)). The final large RMC-refined models show similarly large contributions of the ring fragments. We show the DFT model here for clarity because of its smaller size. As one might expect, the presence of the Ti atoms produced $TaTiO_2$ ring fragments as shown in Fig. 5 (c), in accordance with previous observations of Ti substituting for Ta in Ta/Ti oxides [25, 26]. The $TaTiO_2$ ring fragments became

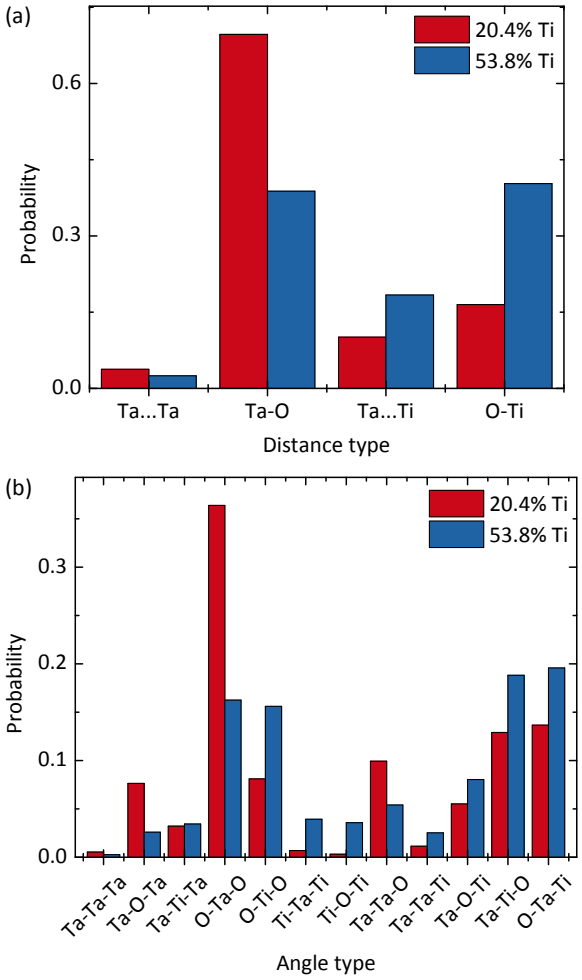

Fig. 4: Parameter probability distributions comparing the 20.4% and 53.8% Ti coatings: (a) bonded and non-bonded distance type distribution; (b) angle type distribution.

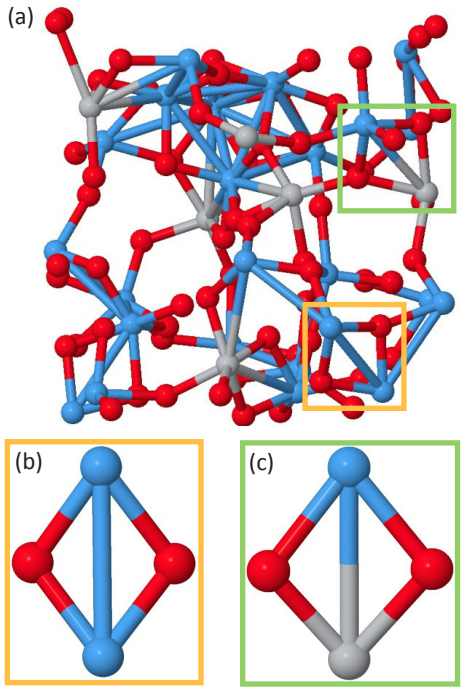

Fig. 5: Image of 20.4% Ti doped coating model for the (a) DFT model highlighting the (b) Ta_2O_2 ring fragments and (c) $TaTiO_2$ ring fragments present in the models. Blue, grey and red atoms are tantalum, titanium and oxygen atoms, respectively.

a more prominent feature in the 53.8% Ti doped coating as a consequence of the increased Ti content. A small number of Ti_2O_2 ring fragments were also present in the coatings, although the Ti...Ti distance there did not fall under the bond definition used in this work.

The angle type distributions show clear variations between the two different coatings as discussed above and shown in Fig. 4 (b). It should be noted that in fused silica, the distribution of bond angles has been related to the characteristics of the observed low temperature mechanical loss peak [27], which is believed to arise from thermally activated transitions in asymmetric double well potentials [27, 28]. It is quite possible that similar transitions between structural configurations with small energy barriers separating them may be related to the mechanical loss in the present coatings. It is quite likely that both bond character, as well the bond angle distribution in the ring fragments plays a part in any such process. The bond angle distribution for three different bond types is shown in Fig. 6, and this demonstrates a subtle change between the two coatings. This suggests that bonding in the two compositions is similar in character, even if the proportions of different bonded / non-bonded distance types changes with increased Ti content.

The $TaTiO_2$ ring fragments have Ta...Ti distances that are on average slightly shorter than the Ta...Ta distances present in the Ta_2O_2 ring fragments. This is also reflected in the angle distributions, especially those of metal-oxygen-metal bond angles. Fig. 6 shows the (a) Ta-O-Ta, (b) Ta-O-Ti and (c) Ti-O-Ti bond angle distributions. Ta-O-Ta and Ti-O-Ti bonds angles appear to have similar angular distributions, peaking around 130-140 °, even if the latter bonds are rather rare, especially in the 20.4% Ti doped coating. On the other hand, Ta-O-Ti bonds seem to have a rather smaller most frequently occurring angle, peaking around 110-120 °, suggesting a rather closer approach of the Ta and Ti atoms across the $TaTiO_2$ ring fragments than across Ta_2O_2 or Ti_2O_2 rings. For both of these models, the peaks of the Ta-O-Ta and Ta-O-Ti bond angle distributions appears to reduce by around 10 ° as the Ti doping is increased. Support of these conclusions and other trends can be discerned for the other

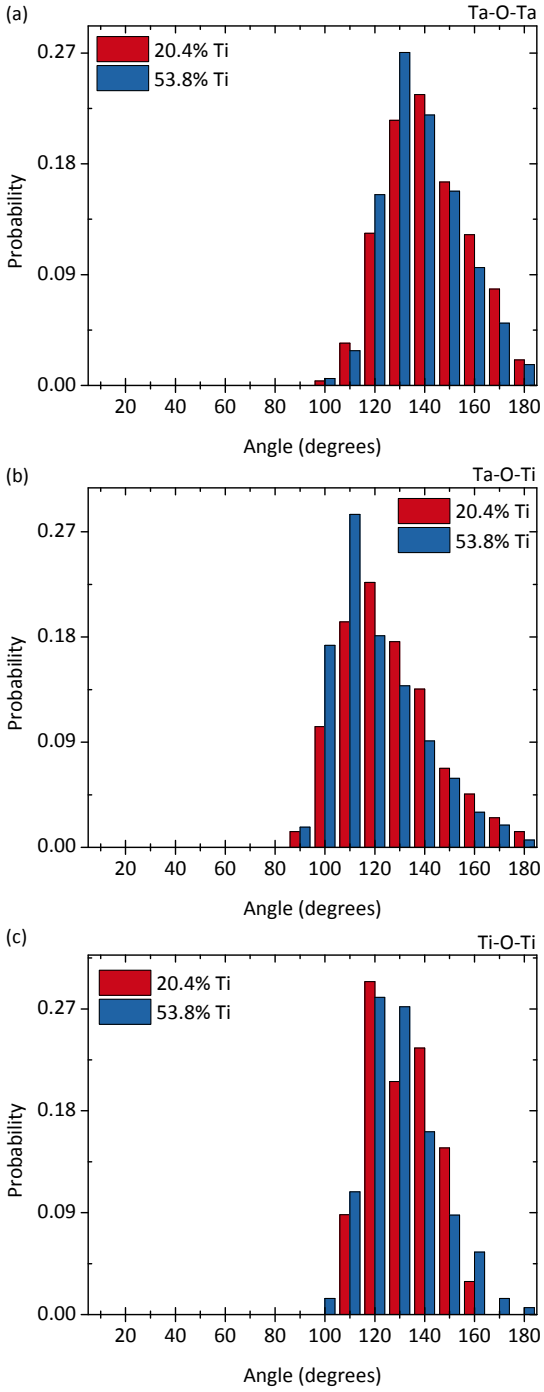

Fig. 6: Angle probability distributions comparing the 20.4% and 53.8% Ti coatings for (a) Ta-O-Ta, (b) Ta-O-Ti and (c) Ti-O-Ti angle types.

possible angle types and these are summarised in the Supplemental material.

5. Discussion: The link between atomic structure and low mechanical loss

The results outlined in the previous sections demonstrate that the lowering of mechanical loss in amorphous Ti doped Ta_2O_5 appears to be well correlated with changes in the atomic structure. Specifically, the width of the first main peak in the Reduced Density Function corresponding to the metal-oxygen nearest neighbour distances correlates very well with the measured mechanical loss. This has the consequence that a high degree of structural homogeneity at the nearest neighbor level is related to a low level of mechanical loss, and that Ti doping promotes this, with an optimum effect around 20-30% Ti. Clearly, the highest degree of such homogeneity can be related to spatial ordering and would be found when a coating is crystallized. However, coatings that have poly-crystalline structures would have internal boundaries with non-optimal atomic structures leading to additional mechanical losses, as well as internal light scattering, and anisotropic optical properties among other deleterious effects. Thus when looking at Ti doped Ta_2O_5 for creating low loss coatings for application in high precision interferometry, the aim is to create as highly homogeneous, and possibly ordered, local structures as are compatible with the amorphous state. It should be noted that epitaxially grown single crystalline coatings, which do not suffer from the same detrimental effects to internal losses as poly-crystalline materials, are currently being studied as a possible alternative to traditional amorphous ion-beam-sputtered coatings. Additionally, it should be noted that the lowest mechanical loss, 28.3% Ti, coating was also shown to be the least oxygen deficient coating at around 3%, indicating that is the coating closest to a perfect stoichiometry, where for every Ta or Ti atom there were 2.5 or 2 oxygen atoms, respectively, in the atomic structure. This may also be an indication that the amount of oxygen in a coating plays an important role in its mechanical loss and that Ti doping may also be helping to prevent oxygen loss.

Models created using our combined RMC and DFT process show clear simi-

larities between the 20.4% and 53.8% Ti doped coatings with very similar bond types and structural elements present in both materials, and both coatings give a 40% lower mechanical loss than undoped or 8.3% Ti doped tantala, so these models show clearly an atomic structure with intrinsically lower loss than the undoped tantala modelled previously [13]. Nevertheless, there are subtle differences between the two models that may explain why the 20-30% Ti gives the lowest loss in this system. Specifically, a significant fraction of $TaTiO_2$ ring fragments is formed in the 20.4% doped coating where Ti substitutes for a Ta atom in the Ta_2O_2 ring fragment that is frequently observed in amorphous pure Ta_2O_5. This substitution changes the shape of the ring fragment by opening the O-Ti-O angle slightly, and making the Ta-O-Ti angle a little smaller making the overall fragment to appear a little wider. Such a change may have clear effects on the mechanical properties of these commonly observed structural components and it would seem that has something to do with lowering the mechanical loss in the materials, although the precise mechanism is as yet unclear. In contrast to this, in the 53.8% Ti doped sample, there is a significant population of Ti_2O_2 ring fragments, in addition to Ta_2O_2 and $TaTiO_2$ ring fragments, and these have different shapes again. Certainly, the Ti-O-Ti bond angles that would be a key feature of these Ti_2O_2 ring fragments have higher angles in the 53.8% Ti doped sample, suggest thinner and more elongated ring fragments. Such Ti-dominated ring fragments will have different mechanical properties again, leading to different mechanical loss properties in the higher Ti-doped sample. For this reason, the next step on the way towards better understanding of such technologically and scientifically useful optical coating materials would be the ab-initio modelling of the structure and properties of these different key structural units of the TiO_2-Ta_2O_5 system. This is the subject of our ongoing work.

6. Conclusions

We have investigated the structural changes occuring as a result of the doping of amorphous Ta_2O_5 with varying levels of TiO_2 using electron diffraction based Reduced Density Function analysis and have shown clear trends in nearest

neighbour distances and bond homogeneity as a result of the doping. Moreover, nearest neighbour distance homogeneity correlates well with the measured mechanical loss across this doping series, suggesting that the structural changes at this scale may be partially responsible for these trends in mechanical loss behaviour. The structures of two of the samples in the doping series have then been modelled in more detail using a combination of reverse Monte Carlo and Density Functional Theory Molecular Dynamics methods to allow us to probe the atomic structures in more detail. This has revealed that the Ti dopant substitutes very well for the Ta atoms in the building blocks of the structure, but modifies it as it does so. This is reflected in the changes of bond angle distributions. It was concluded that this will have the effect of changing the mechanical properties of the material at the atomic level, which will clearly affect the measured mechanical loss, although further studies are required to elucidate the exact atomic scale mechanisms behind it. Nevertheless, this work illustrates very well that subtle changes in atomic structure at the nearest neighbour scale in amorphous materials is associated with their technologically important macroscopic properties.

7. Acknowledgements

We would like to thank SUPA, the University of Glasgow, STFC (Grant Nos. ST/I001085/1, ST/J000019/1) in the UK, and Stanford University and the NSF (Grant Nos. PHY-07 57896, PHY-10 68596) in the USA for financial support. RB is grateful to SU2P for the provision of an entrepreneurial fellowship and the EPSRC for a DTA PhD studentship. We also thank the Royal Society (RS), for which IWM is in receipt of a RS University Research Fellowship and SR is in receipt of a RS Wolfson Merit Award. The authors are thankful to Prof. Hai-Ping Cheng at the University of Florida - Gainesville for helpful discussions. We would also like to thank our colleagues in the LSC and Virgo collaborations for their interest in this work. We also wish to acknowledge the use of the Chemical Database Service based at the Daresbury Science and Innovation Campus.

[1] Andrews D, Roden S, King T. IEEE J Quantum Elect 1995;31(9):1709 –1715.

[2] Numata K, Kemery A, Camp J. Phys Rev Lett 2004;93:250602.

[3] Jiang YY, Ludlow AD, Lemke ND, Fox RW, Sherman JA, Ma LS, et al. Nat Photonics 2011;5(3):158–161.

[4] Harry GM, the LIGO Scientific Collaboration . Classical Quant Grav 2010;27(8):084006.

[5] Harry GM, Armandula H, Black E, Crooks DRM, Cagnoli G, Hough J, et al. Appl Opt 2006;45(7):1569–1574.

[6] Saulson PR. Phys Rev D 1990;42:2437–2445.

[7] Harry GM, Abernathy MR, Becerra-Toledo AE, Armandula H, Black E, Dooley K, et al. Classical Quant Grav 2007;24(2):405.

[8] Martin IW, Chalkley E, Nawrodt R, Armandula H, Bassiri R, Comtet C, et al. Classical Quant Grav 2009;26(15):155012.

[9] Martin IW, Bassiri R, Nawrodt R, Fejer MM, Gretarsson A, Gustafson E, et al. Classical Quant Grav 2010;27(22):225020.

[10] Harry G, Bodiya TM, De Salvo R. Optical Coatings and Thermal Noise in Precision Measurement. Cambridge University Press; 2012.

[11] Crooks DRM, Cagnoli G, Fejer MM, Gretarsson A, Harry G, Hough J, et al. Classical Quant Grav 2004;21(5).

[12] Ayache J, Beaunier L, Boumendil J, Ehret G, Laub D. Sample Preparation Handbook for Transmission Electron Microscopy. Springer New York; 2010.

[13] Bassiri R, Borisenko KB, Cockayne DJH, Hough J, MacLaren I, Rowan S. Appl Phys Lett 2011;98(3):031904.

[14] Cockayne DJ. Ann Rev Mater Res 2007;37(1):159–187.

[15] Clark SJ, Segall MD, Pickard CJ, Hasnip PJ, Probert MIJ, Refson K, et al. Z Kristallogr 2005;220:567–570.

[16] Perdew JP, Burke K, Ernzerhof M. Phys Rev Lett 1996;77:3865–3868.

[17] Swallen S, Ediger M. Soft Matter 2011;7(21):10339–10344.

[18] Martyna GJ, Klein ML, Tuckerman M. J Chem Phys 1992;97(4):2635–2643.

[19] Aleshina L, Loginova S. Crystallogr Rep 2002;47(3):415–419.

[20] Stephenson NC, Roth RS. Acta Crystallogr B 1971;27:1037–1044.

[21] Horn M, Schwerdtfeger CF, Meagher EP. Z Kristallogr 1972;136(3-4):273–281.

[22] Zhang RZ, Wang CL, Li JC, Zhang JL, Yang K, Zhang C, et al. Appl Phys Lett 2007;91(9):092909.

[23] Liu XQ, Han XD, Zhang Z, Ji LF, Jiang YJ. Appl Phys Lett 2007;90(21):211904.

[24] Makovec D, Zuo JM, Twesten R, Payne DA. J Solid State Chem 2006;179(6):1782 – 1791.

[25] Kawaguchi H, Matsuo T. J Organomet Chem 2005;690(23):5333–5345.

[26] Castellano B, Solari E, Floriani C, Re N, Chiesi-Villa A, Rizzoli C. Chem-Eur J 1999;5(2):722–737.

[27] Anderson OL, Bömmel HE. J Am Ceram Soc 1955;38(4):125–131.

[28] Wiedersich J, Adichtchev SV, Rössler E. Phys Rev Lett 2000;84(12):2718–2721.

Correlations between the mechanical loss and atomic structure of amorphous TiO_2 doped Ta_2O_5 coatings

R. Bassiri[a,b,*], K. Evans[a], K.B. Borisenko[c], M.M. Fejer[b], J. Hough[a], I. MacLaren[a], I.W. Martin[a], R.K. Route[b], S. Rowan[a]

[a] *SUPA, School of Physics and Astronomy, University of Glasgow, University Avenue, Glasgow G12 8QQ, UK*
[b] *E. L. Ginzton Laboratory, Stanford University, Stanford, California 94305, USA*
[c] *Department of Materials, University of Oxford, Parks Road, Oxford OX1 3PH, UK*

Abstract

Highly reflective dielectric mirror coatings are critical components in a range of precision optics applications including frequency comb techniques, optical atomic clocks, precision interferometry and ring laser gyroscopes. A key limitation to the performance in these applications is thermal noise, arising from the mechanical loss of the coatings. The origins of the mechanical loss from these coatings is not well understood.

Recent work suggests that the mechanical loss of amorphous Ta_2O_5 coatings can drop by as much as 40 % when it is doped with TiO_2. We use a combination of electron diffraction data and atomic modeling using molecular dynamics to probe the atomic structure of these coatings, and examine the correlations between changes in the atomic structure and changes in the mechanical loss of these coatings. Our results show the first correlation between changes in the mechanical loss and experimentally measured changes in the atomic structure resulting from variations in the level of TiO_2 doping in TiO_2 doped Ta_2O_5 coatings, in that increased homogeneity at the nearest neighbour level appears to correlate with reduced mechanical loss. It is demonstrated that subtle but measurable changes in the nearest neighbour homogeneity in an amorphous material can correlate with significant changes in macroscopic properties.

Supplementary Material

Parameters used for extracting the mechanical loss of the tantala/titania coating component

The parameters used for extracting the mechanical loss of the tantala/titania component of the titania doped tantala coatings are given in Table S 1. A description of how similar calculations are carried out is described by Crooks et al [1]. Thicknesses for the individual coating layers of titania doped tantala and silica were calculated assuming a $\lambda/4$ thickness, where $\lambda = 1064$ nm and is based on the wavelength of the laser light used in the LIGO interferometers.

Statistical analysis of the reduced density functions (RDFs)

The observed changes in the RDFs are highlighted by tracking the most important changes between the average RDF for each Ti doped coating where, excluding any data below 1 Å regarded as noise, the first and second major peak positions, heights and full width at half maxima (FWHMs) are measured and shown in Fig. S 1. Fig. S 1 (a) and (b) highlight the changes in the position (r(Å)) of the first peak and second peaks, respectively, and show that the first peak position moves from a minimum at 20.4% Ti doping to a maximum at 28.3% Ti doping, and the second peak has a minimum at 8.3% and a similar maximum at 28.3% Ti doping. Interestingly, both the first and second peak positions show similar patterns of change with increasing Ti doping, both with maximum values for the 28.3% Ti coating, indicating that the metal-oxygen

*Corresponding author
Email address: rbassiri@stanford.edu (R. Bassiri)

Parameters for loss extraction calculation		
Ti Cat %	total coating loss	refractive index
0	3.0E-4	2.07
8.3	2.7E-4	2.08
20.4	1.9E-4	2.09
25.71	2.0E-4	2.07
28.3	1.7E-4	2.12
53.76	2.10E-4	2.18
SiO_2 refractive index	1.48	
TiO_2 bulk modulus	290 GPa	
Ta_2O_5 bulk modulus	140 GPa	

TABLE. S 1: Parameters used in calculating the tantala/titania components of the titania doped tantala coatings

and metal···metal distances are furthest apart at the 28.3% Ti coating. Fig. S 1 (c) shows that the first peak height (G(r)) has a generally increasing trend as Ti doping increases, indicating an increasing probability of finding the nearest neighbour distances of Ta-O or Ti-O at the peak maximum. This is further supported by evidence that the peaks are becoming narrower as Ti doping increases, as shown when examining the FWHM of the peak (Fig. S 1 (e)), indicating a decrease in distance distribution. Fig. S 1 (d) shows that the second peak height increases from 0% Ti doping until a maximum at around 20% Ti doping and then decreases with increasing Ti doping. At the same time, Fig. S 1 (f) shows that the peak width increases with increasing Ti doping. This change in shape is likely due to the increased variety of interactions that make up the second peak from Ta···Ta and Ta···Ti or Ti···Ti distances when Ti doping is present.

Angle distribution trends in the coating atomic models

The conclusions made from the angle distributions described in Section 5 of the main paper are further supported by the analysis of oxygen-metal-oxygen bond angles in the coatings, i.e., the O-Ta-O and O-Ti-O bond angle distribution shown in Fig. S 2 (a) and (b), respectively. Whilst the peak of the O-Ta-O bond angle distribution lies in a similar place, there is a wider distribution and a larger high angle tail for O-Ti-O angles, which probably also corresponds to the $TaTiO_2$ ring fragments, and this trend is also apparent in the O-Ti-O bond angle distribution.

Furthermore, the Ta-Ta-O (Fig. S 2 (c)) and the Ta-Ti-O (Fig. S 2 (d)) bond angle distributions both show a defined peak at 30 ° and 40 ° relating to the ring fragments, which in both cases become more defined as the Ti doping increases. The Ti-Ta-Ti bond angles (Fig. S 2 (e)) show the range of all metal bond angles, with a peak at around 70-80 ° and there appears to be more of a spread at higher angles as Ti doping increases.

[1] Crooks DRM, Cagnoli G, Fejer MM, Gretarsson A, Harry G, Hough J, et al. Classical Quant Grav 2004;21(5):S1059.

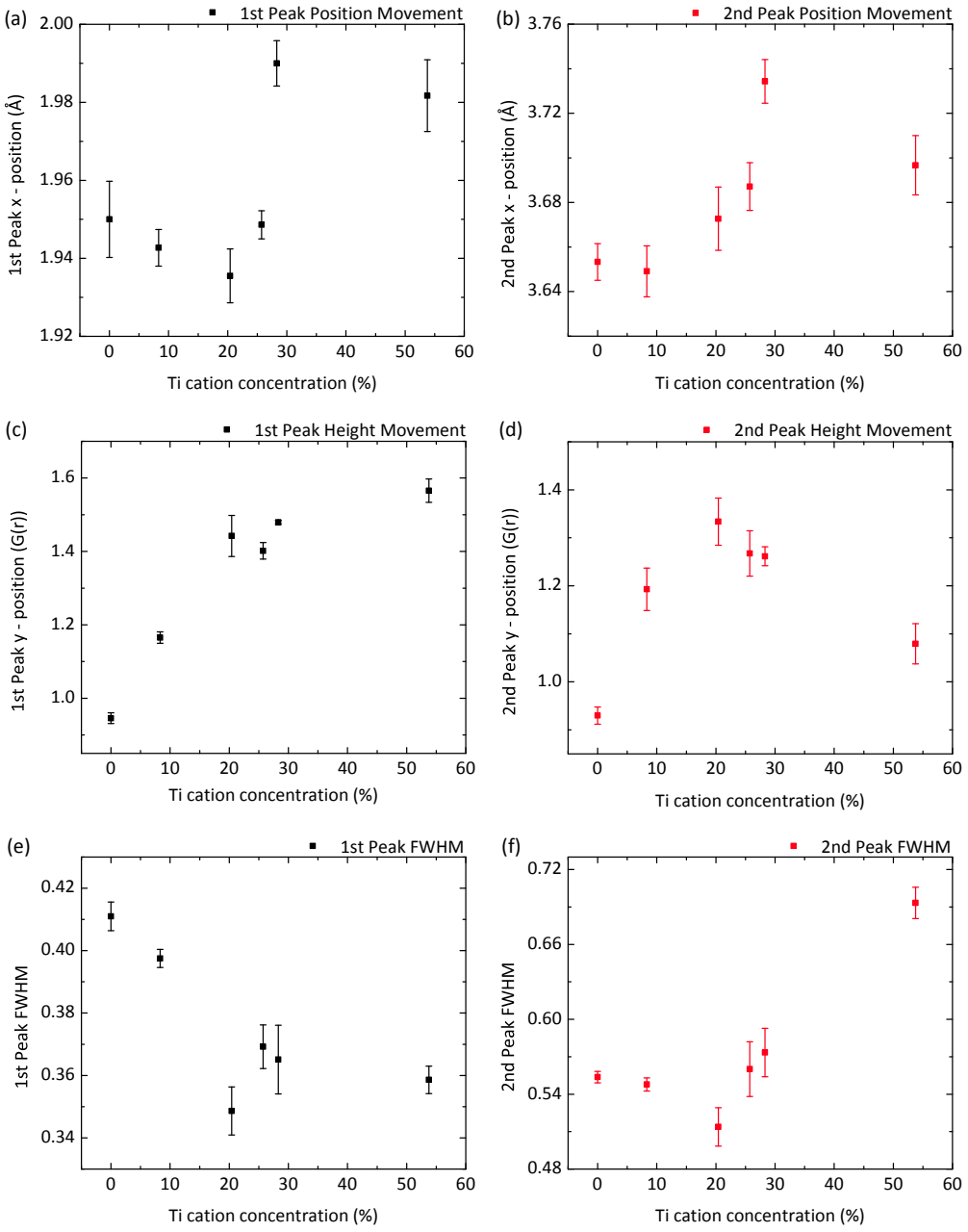

Fig. S 1: RDF analysis of the doped Ta_2O_5 coatings, where the changes in the RDFs against depth into the coating are presented. (a) and (b) show the changes to the 1st and 2nd major peak positions, (c) and (d) show changes in the 1st and 2nd peak heights respectively, and (e) and (f) shows the changes in the 1st and 2nd peak full width half maxima respectively.

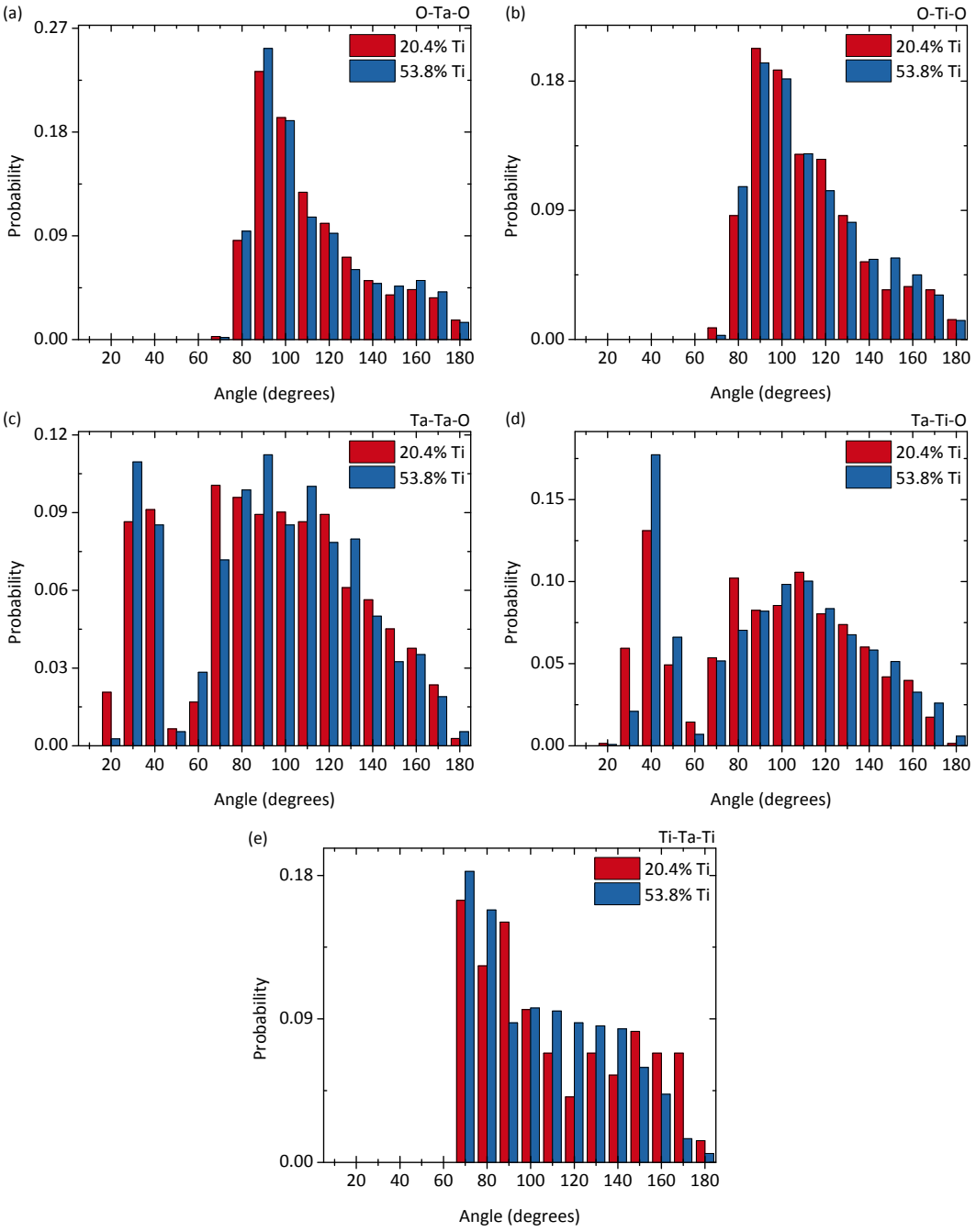

Fig. S 2: Angle distributions comparing the 20.4% and 53.8% Ti coatings for the labelled angle types.